Trends in bulk compressibility of $Mo_{2-x}W_xBC$ solid solutions

Marcus E. Parry,[†] Jackson Hendry,[†] Samantha Couper,[‡] Aria Mansouri Tehrani,[¶] Anton O. Oliynyk,[¶] Jakoah Brgoch,[¶] Lowell Miyagi,[‡] and Taylor D. Sparks[*,†]

[†]*Department of Materials Science and Engineering, University of Utah, Salt Lake City, Utah 84112, United States*

[‡]*Department of Geology and Geophysics, University of Utah, Salt Lake City, Utah 84112, United States*

[¶]*Department of Chemistry, University of Houston, Houston, Texas 77204, United States*

E-mail: sparks@eng.utah.edu

Abstract

The $Mo_{2-x}W_xBC$ system is of interest as a material with high hardness while maintaining moderate ductility. In this work, synchrotron diffraction experiments are performed on $Mo_{2-x}W_xBC$ solid solutions, where x = 0, 0.5, and 0.75, upon hydrostatic compression to ∼54 GPa, ∼55 GPa, and ∼60 GPa, respectively. Trends in bulk modulus, K_0, are evaluated by fitting collected pressure-volume data with a third-order Birch-Murnaghan equation of state, finding K_0 = 333(9) GPa for Mo_2BC, K_0 = 335(11) GPa for $Mo_{1.5}W_{0.5}BC$, and K_0 = 343(8) GPa for $Mo_{1.25}W_{0.75}BC$. While K_0 demonstrates a slight increase when Mo is substituted by W, calculated zero pressure unit cell volume, V_0, exhibits the opposite trend. The decrease in V_0 corresponds to an increase in valence electron density, hardness, and K_0. Observations corroborate previously reported computational results and will inform future efforts to design sustainable materials with exceptional mechanical properties.

Introduction

The automotive, aerospace, defense, and health care industries, among others, depend on materials with enhanced hardness.[1] Efforts to discover superhard materials, with a Vickers hardness (H_V) $\geq$ 40$\tilde{\text{G}}$Pa, have largely relied upon simple design rules and trial-and-error approaches.[2] Accordingly, attempts to mimic the structural and mechanical properties of diamond ($H_V \approx 90 - 100\tilde{\text{G}}$Pa), the prototypical superhard material, have manipulated light, main group elements to achieve the desired strong, dense 3D network of short covalent bonds.[3–6] Cubic boron nitride (c-BN, $H_V = 55$ GPa) and BC_2N ($H_V = 65$ GPa) are examples of this type.[7–9] However, the synthesis of diamond and other hard materials in its class is often cost-prohibitive, requiring extreme temperatures and pressures.[2] To combat the exorbitant synthetic costs, researchers have directed focus towards another class of hard materials: transition metal (TM) borides such as ReB_2 ($H_V = 45$ GPa) and WB_4 ($H_V = 43$ GPa).[10,11] Integration of the TMs simplifies material synthesis because conventional arc melting processes can yield the desired structures. In these structures, the light boron atoms support the formation of covalent bonding networks, while the heavy TMs are intrinsically incompressible due to their high valence electron density, properties well understood to promote hardness.[1,3,12]

Incorporating TMs into superhard materials discovery efforts unearths a vast, underexplored compositional space and provides an excellent opportunity to investigate new materials compositions with optimized mechanical properties. Although superhard materials of this type are often impractical as candidates for industrial use as the TMs employed can be expensive and scarce, sustainability concerns can be addressed through elemental substitution of the expensive, rare-earth TMs with more earth-abundant metals.[2] TM substitution can also modify valence electron concentration (VEC) and atomic size effects to tailor mechanical properties. For instance, substitution of W with Ti, Zr, Hf, Mo, Ta, Mn, or Cr improves hardness of WB_4-based solid solutions from $H_V = 43$ GPa to greater than $H_V = 50$ GPa.[13–15] Similarly, $Mo_{0.9}W_{1.1}BC$ demonstrates improved hardness compared to

its isostructural parent composition, Mo_2BC, with $H_V = 26.5$ GPa and $H_V = 42.1$ GPa, respectively, at 0.49 N indentation load.[16]

The $Mo_{2-x}W_xBC$ solid solution system is of particular interest because it provides the unique opportunity to optimize hardness while maintaining moderate ductility, contradictory extrinsic properties often challenging to predict and control. Although hardness and ductility are difficult to predict directly, bulk modulus (K) and shear modulus (G) are intrinsic material properties that correlate to ductility, brittility, and hardness, allowing for indirect estimations. Pugh's ratio, G/K, estimates ductility in inorganic compounds, as compounds with $G/K < 0.57$ are considered ductile and those ≥ 0.57 brittle.[17] The elastic moduli of hard, isostructural MoWBC and Mo_2BC have been investigated using density functional perturbation theory, finding $G/K = 0.579$ and 0.576, respectively.[16] Thus, it is suggested that ductility is preserved in the $Mo_{2-x}W_xBC$ system regardless of the TM ratio, even though elemental substitution of Mo with W results in increased hardness. A separate *ab initio* study of Mo_2BC also suggests moderate ductility due to the presence of both the metallic interlayer bonding and stiff carbide and boride layers.[18] The ability to maintain ductility in high-hardness materials is an intriguing concept as conventional superhard materials are typically brittle (i.e. diamond $G/K = 1.21$).[19]

Experimental determination of trends in K within $Mo_{2-x}W_xBC$ solid solutions is a pragmatic step towards informing computational efforts and developing an improved understanding of the balance between elastic moduli, hardness, and ductility in TM-based hard, incompressible materials. Bulk compressibility can be determined through *in situ* hydrostatic compression experiments in the diamond anvil cell (DAC). In this process, synchrotron diffraction patterns are incrementally collected upon compression, monitoring changes in lattice parameters and fitting an equation-of-state (EOS) to the resultant relative cell volume versus pressure curves. DAC experiments on the tungsten-rich composition, $Mo_{0.9}W_{1.1}BC$, revealed its ultraincompressibility with $K = 373$ GPa.[20] This work investigates trends in hydrostatic compressibility of other $Mo_{2-x}W_xBC$ solid solutions, where $x = 0$, 0.5, and 0.75, to eluci-

date correlations among composition manipulation and physical and mechanical properties of *TM*-based, hard, incompressible materials. Results will inform future materials design efforts in the quest to optimize mechanical properties while considering synthetic accessibility and material sustainability, providing significant opportunity for applications requiring wear-resistant, superhard materials.

Experimental Methods

Three isostructural $Mo_{2-x}W_xBC$ compositions, where $x = 0$, 0.5, and 0.75, were synthesized in a previous work.[16] Stoichiometric ratios of the starting materials, including Mo (Alfa Aesar, 99.95%), W (Alfa Aesar, 99.5%), crystalline B (Alfa Aesar, 99.5%), and graphite (Sigma-Aldrich, 99.99%), were weighed out to a total mass of 0.25 g and pressed into 6 mm pellets. The pellets were arc melted in a flowing argon atmosphere on a water-cooled copper hearth, flipping each sample at least twice to ensure homogeneous melting and thorough mixing of the elements.

To evaluate bulk compressibility, synchrotron diffraction experiments were performed on each $Mo_{2-x}W_xBC$ composition under compression. A Diamonite^{TM} mortar and pestle was used to grind the arc melted samples to a fine powder, mixing in 5% ruby powder and 10% platinum powder as pressure calibrants.[21] The finest particles were isolated from the bulk powder through solvent suspension in methanol. This process was repeated on the isolated material to achieve an even finer particle size. Sample/Pt mixtures were loaded into a 45-60 μm diameter sample chamber which was laser milled into stainless steel gasket material after pre-indention to a thickness of $\sim$40 μm from an initial thickness of 250 μm. To achieve near-hydrostatic conditions, sample mixtures were gas loaded into the sample chamber with a neon pressure medium. High pressure conditions were achieved using a symmetric DAC with 200 μm diameter flat culet diamond anvils.

Facilities of the High Pressure Collaborative Access Team (HPCAT) at beamline sector

16-ID-B of the Advanced Photon Source (APS) were used to perform the synchrotron experiments. The $Mo_{2-x}W_xBC$ samples were incrementally compressed to ∼55-60 GPa in steps of 1-5 GPa at ambient temperature. At each step, monochromatic X-rays ($\lambda = 0.4066$ Å) and a Pilatus detector were used to collect angle-dispersive diffraction spectra in axial geometry. X-ray energy was ∼30.5 keV and the beam was focused to 5 μm × 4 μm. A cerium dioxide standard was used to calibrate sample-to-detector distance (209.7 mm), detector tilt, and detector rotation. Collected 2D diffraction images were converted from polar coordinates to Cartesian coordinates using FIT2D.[22] Lattice parameters were determined from the diffraction data using the Le Bail method as implemented in the MAUD (Materials Analysis Using Diffraction) software package.[23] Because near-hydrostatic conditions were maintained, lattice strain was not refined. An isothermal, third-order Birch-Murnaghan EOS (Equation 1) was fit to the relative cell volume versus pressure curves using EOSFit software to determine K_0 and the first pressure derivative of the bulk modulus, K_0'.[24]

$$P(V) = \frac{3K_0}{2}\left[\left(\frac{V_0}{V}\right)^{\frac{7}{3}} - \left(\frac{V_0}{V}\right)^{\frac{5}{3}}\right]\left[1 + \frac{3}{4}(K_0' - 4)\left[\left(\frac{V_0}{V}\right)^{\frac{2}{3}} - 1\right]\right] \quad (1)$$

Results and Discussion

To determine K_0 of three $Mo_{2-x}W_xBC$ solid solutions (x= 0, 0.5, 0.75), synchrotron diffraction patterns were collected upon hydrostatic DAC compression. The diffraction data were evaluated using MAUD software, refining lattice parameters of both the borocarbides and internal platinum pressure calibrant to monitor pressure.[21,23] Mo_2BC, $Mo_{1.5}W_{0.5}BC$, and $Mo_{1.25}W_{0.75}BC$ were compressed to ∼54 GPa, ∼55 GPa, and ∼60 GPa, respectively, as determined by the platinum EOS. Refined lattice parameters, associated error, and calculated pressure values are presented in Tables 1-3. Figure 1 illustrates the diffraction data as an intensity map for each $Mo_{2-x}W_xBC$ solid solution, demonstrating compression of the crystal structure as peaks shift to higher Q-space values with increasing pressure. In all of the

Table 1: Refined lattice parameters for Mo_2BC and the associated Pt pressure calibrant with calculated pressure values.

	Mo_2BC			Pt	
R_{wp}	a (Å)	b (Å)	c (Å)	a (Å)	P (GPa)
1.60	3.0803(1)	17.3113(6)	3.03997(8)	3.9170(1)	1.30(3)
1.76	3.06614(9)	17.2487(7)	3.03209(9)	3.9034(1)	4.35(3)
1.96	3.0583(1)	17.1992(9)	3.0224(1)	3.8916(3)	7.12(6)
1.89	3.0492(2)	17.156(1)	3.0136(1)	3.8770(2)	10.72(6)
1.35	3.0411(1)	17.1169(7)	3.00919(8)	3.8686(2)	12.90(6)
1.24	3.0345(1)	17.0682(9)	3.0016(1)	3.8574(1)	15.93(4)
1.48	3.0305(1)	17.0401(9)	3.0000(1)	3.8521(2)	17.40(5)
1.35	3.0242(1)	17.052(1)	2.9958(1)	3.8481(2)	18.51(6)
1.83	3.0173(3)	16.997(2)	2.9860(3)	3.8347(2)	22.44(6)
1.33	3.0103(2)	16.990(1)	2.9760(2)	3.8250(2)	25.40(6)
1.16	3.0023(1)	16.9199(9)	2.9704(1)	3.8149(2)	28.61(5)
1.47	2.9924(1)	16.886(1)	2.9622(1)	3.8026(3)	32.7(1)
1.45	2.9848(2)	16.855(1)	2.9595(1)	3.7955(3)	35.2(1)
1.37	2.9757(1)	16.827(1)	2.9470(1)	3.7848(2)	38.95(7)
1.30	2.9710(2)	16.799(1)	2.9427(2)	3.7787(2)	41.20(7)
1.13	2.9641(2)	16.754(1)	2.9340(1)	3.7720(2)	43.73(7)
1.18	2.9613(2)	16.713(1)	2.9276(2)	3.7663(2)	45.93(8)
1.14	2.9567(2)	16.703(1)	2.9259(2)	3.7605(2)	48.21(9)
1.13	2.9512(2)	16.679(1)	2.9215(20	3.7547(2)	50.56(9)
1.20	2.9487(2)	16.668(1)	2.9135(2)	3.7467(2)	53.86(7)
1.29	2.9479(2)	16.665(1)	2.9118(2)	3.7454(2)	54.41(7)

collected spectra, observed peaks could be indexed to either the orthorhombic borocarbide phase or to the platinum or ruby internal pressure calibrants, with no indication of phase transformations across the entire pressure range.

The refined relative volume (V_0/V) is plotted as a function of calculated pressure for each solid solution in Figure 2, while a third-order Birch-Murnaghan EOS (Equation 1) is fit to each dataset to determine V_0, K_0, and K_0'.[24] Table 4 presents the experimentally determined V_0, K_0, and K_0' for each of the three solid solutions, as well as values for a $Mo_{0.9}W_{1.1}BC$ composition from a previous work and DFT and *ab initio* calculated values for MoWBC and Mo_2BC from other sources.[16,18,20] Figure 3 portrays the observed V_0 and K_0 as a function of W-content.

Table 2: Refined lattice parameters for $Mo_{1.5}W_{0.5}BC$ and the associated Pt pressure calibrant with calculated pressure values.

	$Mo_{1.5}W_{0.5}BC$			Pt	
R_{wp}	a (Å)	b (Å)	c (Å)	a (Å)	P (GPa)
1.61	3.0790(1)	17.3141(9)	3.0384(1)	3.9183(2)	1.04(4)
1.76	3.0772(2)	17.2838(8)	3.0333(1)	3.9138(2)	2.01(4)
1.73	3.0658(1)	17.2434(6)	3.0244(1)	3.9014(2)	4.82(5)
1.44	3.0606(2)	17.212(1)	3.0165(2)	3.8917(2)	7.10(4)
1.43	3.0493(2)	17.1460(9)	3.0106(2)	3.8776(2)	10.56(4)
1.51	3.0382(2)	17.110(1)	3.0034(2)	3.8667(2)	13.40(6)
1.35	3.0335(2)	17.0388(9)	2.9970(2)	3.8523(2)	17.34(5)
1.51	3.0247(2)	17.028(1)	2.9883(2)	3.8416(2)	20.39(6)
1.34	3.0223(2)	17.011(1)	2.9831(2)	3.8365(2)	21.91(5)
1.49	3.0168(1)	16.9365(8)	2.9761(1)	3.8250(2)	25.41(7)
1.39	3.0136(2)	16.927(1)	2.9751(2)	3.8221(2)	26.33(6)
1.67	3.0010(2)	16.817(2)	2.9664(2)	3.8075(3)	31.05(9)
1.68	3.0010(2)	16.812(2)	2.9613(2)	3.8057(3)	31.7(1)
1.40	2.9893(2)	16.847(2)	2.9608(2)	3.8004(2)	33.45(9)
1.12	2.9838(2)	16.830(2)	2.9504(2)	3.7904(2)	36.96(6)
1.14	2.9804(2)	16.829(1)	2.9471(2)	3.7862(2)	38.47(6)
1.06	2.9778(2)	16.786(2)	2.9439(2)	3.7799(2)	40.76(7)
1.04	2.9786(3)	16.675(2)	2.9367(3)	3.7725(2)	43.55(7)
1.07	2.9650(2)	16.680(2)	2.9257(2)	3.7624(2)	47.47(8)
1.28	2.9590(2)	16.671(2)	2.9226(2)	3.7534(2)	51.08(8)
1.06	2.9474(2)	16.661(2)	2.9191(2)	3.7443(2)	54.90(7)

To evaluate correlations among composition and the observed trends in bulk moduli and other mechanical properties, it is important to first consider the $Mo_{2-x}W_xBC$ ($0 \leq x < 1.1$) crystal structure. The unit cell is highly anisotropic, crystallizing in an orthorhombic space group (*Cmcm*) isostructural to the Mo_2BC parent phase, and visualized in Figure 4 using VESTA software.[25] Boron atoms are bound together in chains extending in the [001] direction, while the two crystallographically independent *TM* sites (Wyckoff 4*c*) are occupied by a statistical mixing of Mo and W. Compared to other superhard materials, the $Mo_{2-x}W_xBC$ solid solution is somewhat uniquely able to maintain ductility with $G/K \approx 0.57$, at the border of ductility/brittleness, attributed to balance between stiff carbide and boride layers and the metallic interlayer bonding.[16,17]

Table 3: Refined lattice parameters for $Mo_{1.25}W_{0.75}BC$ and the associated Pt pressure calibrant with calculated pressure values.

$Mo_{1.25}W_{0.75}BC$				Pt	
R_{wp}	a (Å)	b (Å)	c (Å)	a (Å)	P (GPa)
1.73	3.0742(1)	17.2984(7)	3.0400(1)	3.92050(9)	0.56(2)
1.93	3.06949(8)	17.2690(6)	3.0374(1)	3.9137(1)	2.04(2)
1.78	3.0585(1)	17.2049(7)	3.0273(1)	3.9008(1)	4.94(3)
2.13	3.0428(1)	17.1623(9)	3.0164(1)	3.8812(1)	9.68(4)
1.61	3.0362(1)	17.1107(8)	3.0070(1)	3.8704(1)	12.43(4)
1.84	3.0342(1)	17.0933(7)	3.00377(8)	3.8644(1)	14.03(3)
1.63	3.0263(2)	17.075(1)	2.9949(1)	3.8552(1)	16.54(4)
2.09	3.0193(2)	17.050(1)	2.9918(2)	3.8452(2)	19.35(4)
1.68	3.0227(2)	16.985(1)	2.9886(1)	3.8390(1)	21.16(4)
1.94	3.0014(2)	16.969(1)	2.9699(1)	3.8224(2)	26.23(6)
1.65	2.9988(2)	16.893(1)	2.9665(2)	3.8160(2)	28.28(5)
1.50	2.9894(2)	16.870(1)	2.9555(1)	3.8027(1)	32.67(5)
2.63	2.9836(3)	16.829(2)	2.9494(3)	3.7922(2)	36.31(9)
1.49	2.9777(1)	16.754(1)	2.9404(1)	3.7841(1)	39.23(4)
1.47	2.9721(1)	16.736(1)	2.9384(1)	3.7796(1)	40.88(5)
1.29	2.9643(1)	16.6907(9)	2.9319(1)	3.7712(1)	44.06(4)
1.42	2.9586(1)	16.659(1)	2.9246(1)	3.7632(1)	47.17(5)
1.40	2.9496(1)	16.608(1)	2.9163(1)	3.7501(1)	52.45(5)
1.38	2.9453(1)	16.589(1)	2.9104(1)	3.7442(1)	54.93(5)
1.50	2.9396(1)	16.545(1)	2.9049(1)	3.7360(1)	58.47(6)
1.62	2.9357(1)	16.537(1)	2.9000(1)	3.7333(2)	59.66(7)

Table 4: Experimentally determined V_0, K_0, and K_0' for $Mo_{2-x}W_xBC$ solid solutions, including results reported in a previous work.[20] DFT and *ab initio* calculated values for Mo_2BC and MoWBC are also presented for reference.[16,18]

	3rd-order B-M EOS			DFT[16]	*ab initio*[18]
Composition	V_0	K_0	K_0'	K_0	K_0
Mo_2BC	162.5(1)	333(9)	3.7(4)	328	324
$Mo_{1.5}W_{0.5}BC$	162.3(1)	335(11)	4.1(5)		
$Mo_{1.25}W_{0.75}BC$	161.9(1)	343(8)	3.2(3)		
MoWBC				349	
$Mo_{0.9}W_{1.1}BC$[20]	162.000(3)	373(4)	2.3(2)		

For the experimentally evaluated $Mo_{2-x}W_xBC$ solid solutions, K_0 appears to directly correlate with increasing W content and decreasing Mo content, from K_0 = 333(9) GPa

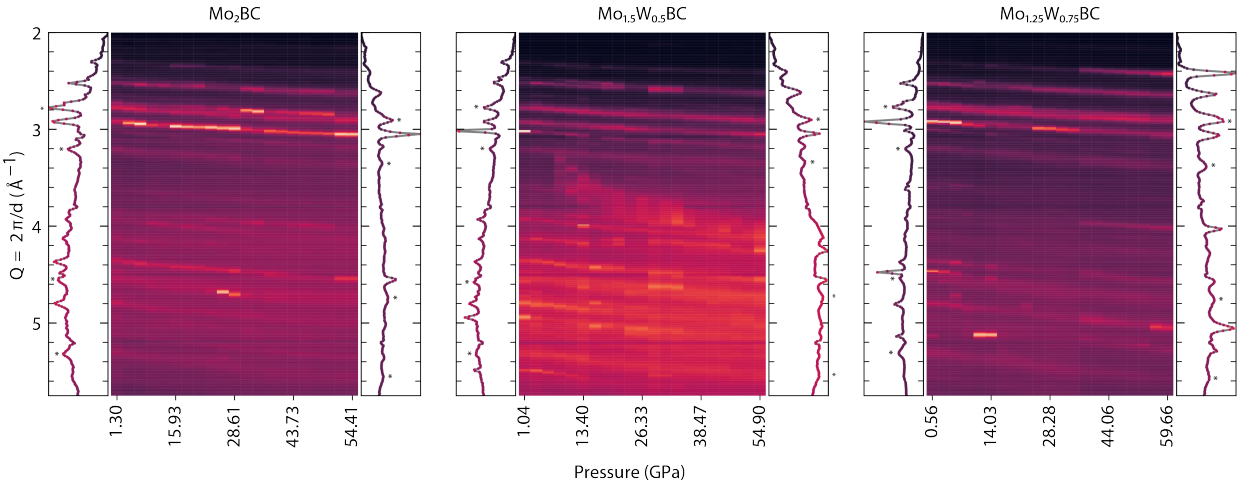

Figure 1: Collected synchrotron diffraction patterns for three $Mo_{2-x}W_xBC$ solid solutions are presented as a heatmap, demonstrating a shift in Q-space with the application of hydrostatic pressure. Platinum pressure calibrant peaks are indicated by $(*)$, while other prominent peaks represent the borocarbide solid solutions.

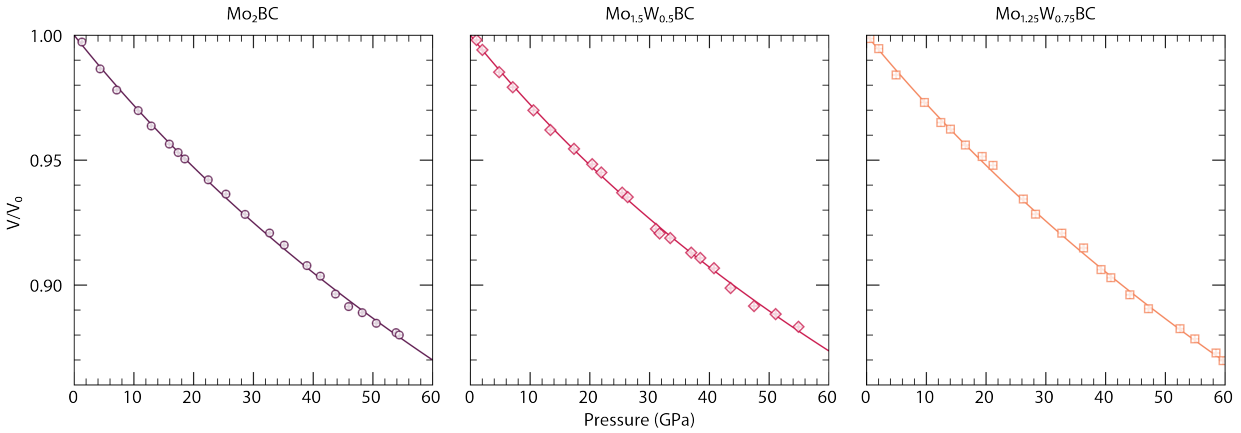

Figure 2: The relative unit cell volume is plotted against pressure for each of the three $Mo_{2-x}W_xBC$ solid solutions, and a 3rd-order Birch-Murnaghan EOS is fit to each dataset. Error bars are smaller than the marker size in each case.

for Mo_2BC to $K_0 = 373(4)$ GPa for $Mo_{0.9}W_{1.1}BC$. These findings indicate that bulk compressibility of the $Mo_{2-x}W_xBC$ structures, particularly the tungsten-rich compositions, are comparable to values reported for WB_4 ($K_0 = 369(9)$ GPa and $K_0' = 1.2(5)$).[26] Additionally, calculated V_0 of $Mo_{2-x}W_xBC$ generally decreases as W content increases, in agreement with X-ray diffraction results reported previously, and can be explained by shorter, stronger bonding among the *TM*s.[16] Reduced crystal volume also correlates to increased valence electron

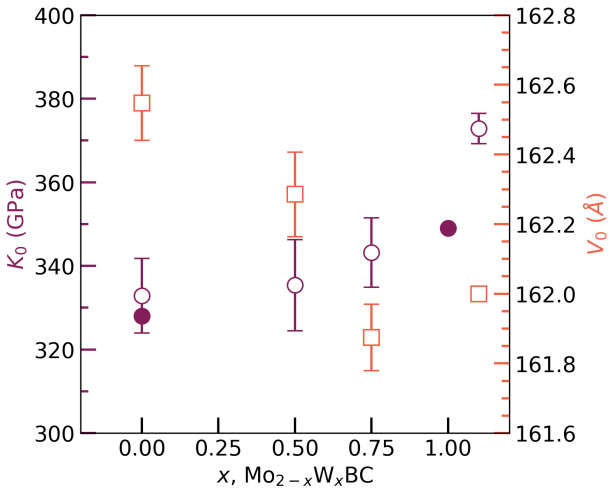

Figure 3: K_0 and V_0 are plotted against x in $Mo_{2-x}W_xBC$. The $Mo_{0.9}W_{1.1}BC$ results are from a previous work.[20] Experimentally determined values are plotted as open markers, while previous DFT calculated K_0 values are plotted as solid markers for comparison.[16]

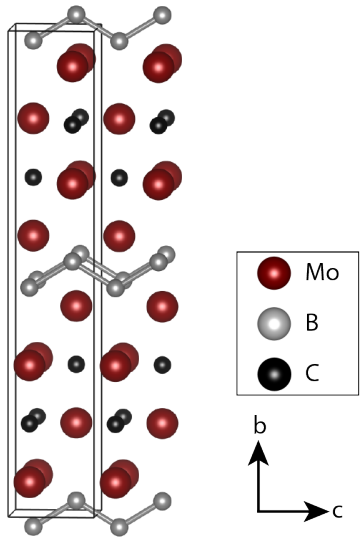

Figure 4: Crystal structure of Mo_2BC, isostructural to the $Mo_{2-x}W_xBC$ solid solutions when $0 \leq x \leq 1.1$.

density, and therefore incompressibility, corroborating the observed trend in K_0. DFT and *ab initio* calculated K_0 for Mo_2BC, reported as $K_0 = 324$ and $K_0 = 328$ by Emmerlich et al. and Mansouri Tehrani et al., respectively, are in good agreement with the experimentally determined value of this work.[16,18] Mansouri Tehrani et al. also report $K_0 = 349$ GPa for MoWBC through DFT calculations. The increase in K_0 upon W substitution for Mo

is consistent with experimental observations here. These results demonstrate the capacity of *TM* substitution to manipulate atomic size effects and valence electron density to tailor mechanical response.

In addition to the exceptional bulk moduli, hardness, and ductility of this system, understanding these properties in the context of the anisotropic lattice strain and texture development when exposed to nonhydrostatic stresses can inform future efforts to implement $Mo_{2-x}W_xBC$ solid solutions in applications requiring wear-resistance. Previously, nonhydrostatic compression experiments on $Mo_{0.9}W_{1.1}BC$ investigated anisotropic deformation behavior and found that the (002) and (200) planes parallel to the long *b*-axis support the greatest differential strain.[27] These planes are orthogonal to the covalently bonded boron chains, which likely provide additional elastic support and decrease the susceptibility to slip. Furthermore, lattice preferred orientation was demonstrated along planes parallel to the covalent chains, suggesting that dislocation glide occurs in directions that do not require the breaking of B–B bonds. Mansouri Tehrani et al. used stress-strain calculations to investigate the anisotropic, nonlinear elastic behavior of Mo_2BC and observed tensile strain stiffening along the [001] direction.[28] The observed stiffening was attributed to the formation of an electronic pseudogap within the density of state and the dimerization of the boron-boron chains, delaying shear failure and enhancing ultimate strength and strain. Additionally, the $(111)[\bar{1}\bar{1}2]$ was identified as the softest shear plane, contributing to the ductility of the structure. Because the $Mo_{2-x}W_xBC$ solid solutions are isostructural, it is anticipated that the deformation mechanisms are similar across this system.

Conclusions

The $Mo_{2-x}W_xBC$ system demonstrates the potential to optimize hardness, ductility, and sustainability in synthetically accessible inorganic materials for applications requiring wear-resistant, superhard materials. In this work, bulk compressibility of $Mo_{2-x}W_xBC$ solid solu-

tions, where x= 0, 0.5, and 0.75, were evaluated through *in situ* hydrostatic, high-pressure synchrotron diffraction experiments to ∼54 GPa, ∼55 GPa, and ∼60 GPa, respectively. The calculated Birch-Murnaghan EOS for each composition demonstrate an increase in K_0 with rising W content and are in good agreement with previous computational studies. Furthermore, V_0 decreases as Mo is substituted by W, corresponding to the increase in valence electron density, hardness, and K_0. Experimental determination of trends in K_0 within $Mo_{2-x}W_xBC$ solid solutions can inform future computational and experimental design endeavors in the search for environmentally sustainable materials with superb mechanical response.

Acknowledgement

The synchrotron experiments were performed at HPCAT (Sector 16), Advanced Photon Source (APS), Argonne National Laboratory. The Advanced Photon Source is a U.S. Department of Energy (DOE) Office of Science User Facility operated for the DOE Office of Science by Argonne National Laboratory under Contract No. DE-AC02-06CH11357. HPCAT operations are supported by DOE-National Nuclear Security Administration's (NNSA) Office of Experimental Sciences. The authors thank Yue Meng for beamline technical support. Financial support was provided by the National Science Foundation through No. NSF-CMMI 15-62226 (T. D. S. and M. P.), No. NSF-CMMI 15-62142 (J. B. and A. M.), and EAR-1654687 (L. M.). A. O. O. gratefully acknowledges the Eby Nell McElrath Postdoctoral Fellowship at the University of Houston for Financial support. L. M. acknowledges support from U.S. DOE-NNSA through the Chicago-DOE Alliance Center which provided financial support for S.C. (DE-NA0003975).

References

(1) Kaner, R. B.; Gilman, J. J.; Tolbert, S. H. Designing Superhard Materials. *Science* **2005**, *308*, 1268–1269.

(2) Mansouri Tehrani, A.; Ghadbeigi, L.; Brgoch, J.; Sparks, T. D. Balancing Mechanical Properties and Sustainability in the Search for Superhard Materials. *Integrating materials and manufacturing innovation* **2017**, *6*, 1–8.

(3) Haines, J.; Léger, J.; Bocquillon, G. Synthesis and Design of Superhard Materials. *Annual Review of Materials Research* **2001**, *31*, 1–23.

(4) Vepřek, S. The search for novel, superhard materials. *Journal of Vacuum Science & Technology A* **1999**, *17*, 2401–2420.

(5) Bundy, F. P.; Hall, H. T.; Strong, H. M.; Wentorfjun, R. H. Man-Made Diamonds. *Nature (London)* **1955**, *176*, 51–55.

(6) Wentorf, R. H.; DeVries, R. C.; Bundy, F. P. Sintered Superhard Materials. *Science* **1980**, *208*, 873–880.

(7) Singh, B.; Solozhenko, V.; Will, G. On the low-pressure synthesis of cubic boron nitride. *Diamond and Related Materials* **1995**, *4*, 1193 – 1195.

(8) Solozhenko, V. L.; Dub, S. N.; Novikov, N. V. Mechanical properties of cubic BC2N, a new superhard phase. *Diamond and Related Materials* **2001**, *10*, 2228 – 2231.

(9) Wentorf, R. H. Synthesis of the Cubic Form of Boron Nitride. *The Journal of Chemical Physics* **1961**, *34*, 809–812.

(10) Chung, H.-Y.; Weinberger, M. B.; Levine, J. B.; Kavner, A.; Yang, J.-M.; Tolbert, S. H.; Kaner, R. B. Synthesis of Ultra-Incompressible Superhard Rhenium Diboride at Ambient Pressure. *Science* **2007**, *316*, 436–439.

(11) Mohammadi, R.; Lech, A. T.; Xie, M.; Weaver, B. E.; Yeung, M. T.; Tolbert, S. H.; Kaner, R. B. Tungsten tetraboride, an inexpensive superhard material. *Proceedings of the National Academy of Sciences* **2011**, *108*, 10958–10962.

(12) Yeung, M. T.; Mohammadi, R.; Kaner, R. B. Ultraincompressible, Superhard Materials. *Annual Review of Materials Research* **2016**, *46*, 465–485.

(13) Akopov, G.; Yeung, M. T.; Turner, C. L.; Mohammadi, R.; Kaner, R. B. Extrinsic Hardening of Superhard Tungsten Tetraboride Alloys with Group 4 Transition Metals. *Journal of the American Chemical Society* **2016**, *138*, 5714–5721.

(14) Mohammadi, R.; Xie, M.; Lech, A. T.; Turner, C. L.; Kavner, A.; Tolbert, S. H.; Kaner, R. B. Toward Inexpensive Superhard Materials: Tungsten Tetraboride-Based Solid Solutions. *Journal of the American Chemical Society* **2012**, *134*, 20660–20668.

(15) Mohammadi, R.; Turner, C. L.; Xie, M.; Yeung, M. T.; Lech, A. T.; Tolbert, S. H.; Kaner, R. B. Enhancing the Hardness of Superhard Transition-Metal Borides: Molybdenum-Doped Tungsten Tetraboride. *Chemistry of Materials* **2016**, *28*, 632–637.

(16) Mansouri Tehrani, A.; Oliynyk, A. O.; Rizvi, Z.; Lotfi, S.; Parry, M.; Sparks, T. D.; Brgoch, J. Atomic Substitution to Balance Hardness, Ductility, and Sustainability in Molybdenum Tungsten Borocarbide. *Chemistry of Materials* **2019**, *31*, 7696–7703.

(17) Pugh, S. XCII. Relations between the elastic moduli and the plastic properties of polycrystalline pure metals. *The London, Edinburgh, and Dublin Philosophical Magazine and Journal of Science* **1954**, *45*, 823–843.

(18) Emmerlich, J.; Music, D.; Braun, M.; Fayek, P.; Munnik, F.; Schneider, J. M. A proposal for an unusually stiff and moderately ductile hard coating material: Mo2BC. *Journal of Physics D: Applied Physics* **2009**, *42*, 185406.

(19) Chen, X.-Q.; Niu, H.; Li, D.; Li, Y. Modeling hardness of polycrystalline materials and bulk metallic glasses. *Intermetallics* **2011**, *19*, 1275–1281.

(20) Mansouri Tehrani, A.; Oliynyk, A. O.; Parry, M.; Rizvi, Z.; Couper, S.; Lin, F.; Miyagi, L.; Sparks, T. D.; Brgoch, J. Machine Learning Directed Search for Ultraincompressible, Superhard Materials. *Journal of the American Chemical Society* **2018**, *140*, 9844–9853.

(21) Fei, Y.; Ricolleau, A.; Frank, M.; Mibe, K.; Shen, G.; Prakapenka, V. Toward an internally consistent pressure scale. *Proceedings of the National Academy of Sciences* **2007**, *104*, 9182–9186.

(22) Hammersley, A. P. *FIT2D*: a multi-purpose data reduction, analysis and visualization program. *Journal of Applied Crystallography* **2016**, *49*, 646–652.

(23) Wenk, H.-R.; Lutterotti, L.; Kaercher, P.; Kanitpanyacharoen, W.; Miyagi, L.; Vasin, R. Rietveld texture analysis from synchrotron diffraction images. II. Complex multiphase materials and diamond anvil cell experiments. *Powder Diffraction* **2014**, *29*, 220–232.

(24) Angel, R. J.; Alvaro, M.; Gonzalez-Platas, J. EosFit7c and a Fortran module (library) for equation of state calculations. *Zeitschrift für Kristallographie - Crystalline Materials* **2014**, *229*, 405 – 419.

(25) Momma, K.; Izumi, F. *VESTA3* for three-dimensional visualization of crystal, volumetric and morphology data. *Journal of Applied Crystallography* **2011**, *44*, 1272–1276.

(26) Xie, M.; Mohammadi, R.; Mao, Z.; Armentrout, M. M.; Kavner, A.; Kaner, R. B.; Tolbert, S. H. Exploring the high-pressure behavior of superhard tungsten tetraboride. *Phys. Rev. B* **2012**, *85*, 064118.

(27) Parry, M.; Couper, S.; Mansouri Tehrani, A.; Oliynyk, A. O.; Brgoch, J.; Miyagi, L.;

Sparks, T. D. Lattice strain and texture analysis of superhard Mo0.9W1.1BC and ReWC0.8via diamond anvil cell deformation. *J. Mater. Chem. A* **2019**, *7*, 24012–24018.

(28) Mansouri Tehrani, A.; Lim, A.; Brgoch, J. Mechanism for unconventional nonlinear elasticity. *Phys. Rev. B* **2019**, *100*, 060102.

Graphical TOC Entry